ACS Electrochemistry

pubs.acs.org/electrochem Article

Tuning Hydrogen Bond Networks at Gold Electrodes: A Study of Potential-Dependent DMSO−Water Interfaces

Saptarsi Mondal, Ziareena A. Al-Mualem, Alfredo E. Cardenas, Sulagna Hazarika, Hyein Lee, Hang Ren, and Carlos R. Baiz*

Cite This: *ACS Electrochem.* 2025, 1, 709−717 Read Online

ACCESS | Metrics & More | Article Recommendations | Supporting Information

ABSTRACT: Manipulating the hydrogen bond (H-bond) networks at metal−solution interfaces is central toward optimizing electrochemical processes. This study investigates the potential-dependent interfacial environment of dimethyl sulfoxide (DMSO)−water mixtures at the gold electrode interface using a combination of surface-enhanced infrared absorption spectroscopy (SEIRAS) and constant-potential molecular dynamics (MD) simulations. SEIRAS provides an *in situ* spectroscopic view of H-bonding populations and cosolvent enrichment at the interface, while MD simulations offer an atomistic view of H-bond populations and molecular orientations under applied potentials. Our results demonstrate that the interfacial H-bonding environment responds to applied electrode polarizations. At negative potentials DMSO becomes enriched at the surface together with a substantial reorientation of interfacial water molecules, leading to a slight increase in H-bond populations, particularly at lower DMSO concentrations. Positive potentials show a reduced impact on the H-bond structure. The effects are different at higher DMSO concentrations where DMSO−DMSO interactions dominate. Our findings therefore suggest that the local H-bond environment at the metal−solution interface can be reshaped with applied electrode charge, even for neutral cosolvents. These insights reveal that a cosolvent like DMSO can be used to optimize catalytic performance by modulating interfacial solvation and proton-coupled electron-transfer pathways.

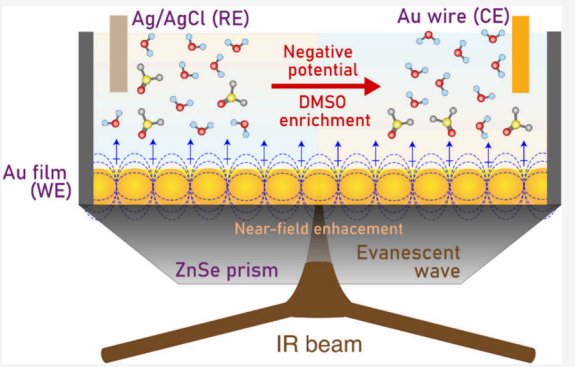

KEYWORDS: *SEIRAS, molecular dynamics, hydrogen bonds, cosolvents, electrochemistry, interface*

INTRODUCTION

The interface between metal surfaces and solutions presents a complex chemical environment. Interfacial regions often exhibit altered reactivity compared to bulk solutions, even in the absence of strong adsorption. This effect arises due to interfacial electric fields,[1,2] modified interfacial H-bonding networks,[3−5] and changes in molecular interactions as a result of altered energetic landscapes.[6] These factors contribute to enhanced or selective reactivity in electrochemical and catalytic systems. Additionally, molecules or ions can adsorb onto the metal surface, thereby modulating the concentration of species and the kinetics of electrocatalytic reactions at the electrode-electrolyte interface. In aqueous solutions, water often serves as both a reactant and a solvent, influencing reactions such as the hydrogen evolution reaction (HER), oxygen reduction reaction (ORR), and the CO_2 reduction reaction.[3,4,7] Understanding the role of interfacial water structure is essential for advancing the understanding of electrocatalytic processes in aqueous media.

The mechanism of HER involves proton-coupled electron transfer to form adsorbed H as the key intermediate, with either H_3O^+ or H_2O as the proton source. In HER, the cathodic half of water splitting by electrolysis, aprotic solvents can tune water−water H-bonds in solution.[7] Since HER under neutral and alkaline conditions relies on water as both a reactant and solvent, optimizing this reaction requires control of the water network at the cathode interface. One promising approach to tune the HER reactivity involves the addition of a cosolvent, which can modulate the hydrogen-bonding environment.[8] The polarity, high water-miscibility, donor−acceptor imbalance, and amphiphilic behavior of dimethyl sulfoxide (DMSO), make DMSO−water cosolvent systems a promising approach to control the local interfacial environment and water network,[9] potentially controlling kinetics and transport in electrocatalytic reactions. DMSO disrupts its local H-bonding environment by acting as a strong hydrogen bond acceptor, forming up to two H-bonds with nearby water molecules.[10−13] Additionally, DMSO molecules form stable dimers via dipole−dipole interactions and hydrophobic methyl group associa-

Received: November 19, 2024
Revised: March 28, 2025
Accepted: April 2, 2025
Published: April 16, 2025

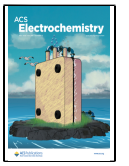

tions.[14−17] These interactions produce microscopic liquid−liquid phase separation that lead to heterogeneous regions enriched in DMSO and regions enriched in water, producing microscopic percolated H-bond networks[10,14] and concentration-dependent solvation dynamics in aqueous systems.[17−25]

We have previously shown that DMSO alters the interfacial hydration environment on gold surfaces.[9] Interfacial DMSO molecules are dehydrated as DMSO is enriched at the Au surface. These changes are accompanied by the formation of water clusters. All-atom molecular dynamics (MD) simulations show a "buckled" conformation of water molecules at the Au surface. This energetically-unfavorable conformation, along with the small cluster sizes, inhibits H-bonding with bulk water, potentially restricting the proton diffusion and transfer necessary for HER.

The structure of the metal/solution interface is governed by the electrical double layer (EDL), which describes how counterions and solvent molecules organize under an applied potential. Classical EDL models, such as the Gouy-Chapman-Stern model, provide a theoretical framework for understanding the distribution of ionic charges, the resulting potential gradients, and their influence on interfacial electric fields.[1,26] At low ionic strengths (∼10 mM), the Debye length (∼3 nm) becomes comparable to the size of molecular dynamics simulation boxes, making it computationally challenging to accurately represent the EDL. However, solvent dipole alignment and hydrogen bonding often dominate interfacial structuring under these conditions, even in the absence of explicit ions.[2,27] This study focuses on how applied potential modulates the molecular configurations and hydrogen-bonding dynamics of DMSO and water at the gold interface, acknowledging the limitations of omitting explicit ionic effects in our simulations. While the effects of DMSO on the electrode interface have been explored, it is necessary to further characterize cosolvent effects under applied electrochemical potentials to understand how interfaces change as potentials approach *in operando* conditions. Specifically, here we aim to understand the effects of applied surface potentials on interfacial DMSO or water enrichment and depletion as well as map out how the applied potential alters DMSO and water configurations at the gold interface.

This study uses a combination of *in situ* experimental spectroelectrochemical measurements using surface-enhanced infrared absorption spectroscopy (SEIRAS) and MD simulations to investigate the local H-bonding networks in water−DMSO cosolvent mixtures on gold electrodes under a range of applied electrostatic potentials. SEIRAS measures interfacial molecular structure and reactions as detection sensitivity is greatly enhanced at metal-liquid interfaces without interference from the bulk phase.[28−31] In SEIRAS, a nanoscale-roughened thin metal film is deposited onto an attenuated total reflectance (ATR) crystal; this metal film serves as the working electrode in electrochemical experiments.[31] The incoming IR beam excites local surface plasmons in the metal film, resulting in a near-field enhancement at the nanometer gaps between the metal nanoparticles. The solvent absorption is minimized from the confined volume of the enhanced electric field.[32,33] SEIRAS provides an ensemble-averaged view of the system, while MD simulations provide a localized atomistic picture of the water network structure and geometry at the metal-liquid interface.

METHODS

Cosolvent Sample Preparation. DMSO−water cosolvent mixtures were prepared for SEIRAS by titrating appropriate volumes of DMSO (≥99.9%, anhydrous; Sigma-Aldrich) into a solution of ultrapure water (Milli-Q) and 20 mol % D_2O (99.9%; Cambridge Isotope Laboratories, Inc.) during the measurements. The mixture compositions were: 0 (no DMSO), 1, 3, 5, 7, 10, 15, 20, 25, 30, 35, and 40 mol % DMSO. The electrolyte was 10 mM $KClO_4$ in ultrapure water. The electrolyte used in this study was 10 mM potassium perchlorate ($KClO_4$), chosen for its weakly adsorbing nature and to minimize competitive effects from ion adsorption on the gold electrode. The low ionic strength (∼10 mM) provides a larger Debye length (∼3 nm), allowing us to probe potential-dependent solvent reorganization with minimal ionic screening. A salt bridge was used to isolate the Ag/AgCl reference electrode from the electrolyte to prevent chloride contamination. Electrolyte solutions were prepared carefully to ensure the absence of residual chloride ions.[34,35] Samples were purged with nitrogen gas prior to measurements. The electrolyte concentration was maintained across all samples.

Gold Surface Preparation for SEIRAS. The gold film for SEIRAS measurement was deposited onto the ZnSe substrate using a previously established electroless deposition method[36] with some modifications as described in the Method section of our earlier work.[9] In brief, the ZnSe ATR prism (60° cut; Pike Technologies) was polished with 1 μm and 0.05 μm alumina slurry then sonicated in ultrapure water for 10 min. The ZnSe crystal was then heated to 50° C and 200 μL of a 25 mM solution of gold(III) chloride trihydrate ($HAuCl_4•3H_2O$) (99.9+%; Sigma-Aldrich) in ultrapure water was dropcasted onto the crystal face and left to deposit for 3 min; this deposition time results in a thicker gold film with a measured penetration depth under 70 nm.[37] The surface was rinsed with water to quench the deposition then dried with a gentle flow of N_2 gas. The gold surface resistance was 0.9 Ω across a ∼1 cm distance on the crystal face.

The electrochemical cell was purged with N_2 gas to remove the interference from O_2. The electrochemical characterization of the Au film was performed using cyclic voltammetry in a N_2-purged 0.1 M phosphate buffer, revealing well-defined Au oxidation and reduction peaks (Figure S50) confirming that the gold film exhibits expected electrochemical behavior. We did not extend the potential window beyond +0.6 V in our measurement to avoid significant oxide formation that can degrade the Au film electrode. Furthermore, we restricted our measurement up to −0.6 V to eliminate ORR/HER reaction that might otherwise interfere with the measurement and influence our interpretation.

Spectroelectrochemical Measurements. SEIRAS measurements were conducted with a Bruker INVENIO Spectrometer equipped with a liquid-nitrogen-cooled mercury−cadmium-telluride (MCT) detector and a Pike Technologies VeeMAX III accessory with the Jackfish J2F electrochemical cell. The Ag/AgCl reference electrode was filled with 3 M KCl. A gold wire was used as the counter electrode. A custom-built LabVIEW data acquisition program was used to synchronize applying a potential with a CH Instruments 1202C potentiostat through the Hard Potato package[38] and collecting the corresponding IR spectra. Prior to data acquisition, the gold surface and electrodes were cleaned in a 10 mM $KClO_4$ in ultrapure water electrolyte solution with >20 CV cycles from

https://doi.org/10.1021/acselectrochem.4c00175
ACS Electrochem. 2025, 1, 709−717

-0.8 to 0.7 V with a 0.1 V/s scan rate (see Figure S49). Each spectrum was averaged from 128 scans with a 2 cm^{-1} spectral resolution. A 10 mM $KClO_4$ electrolyte solution was added to the gold film at 0 V relative to Ag/AgCl (equivalent to 0.198 V vs. the standard hydrogen electrode [SHE]) to correct for solvent effects in the spectra before conducting concentration- and voltage-dependent measurements. The choice of 10 mM $KClO_4$ as the electrolyte allows us to focus on potential-dependent effects on solvent structuring and hydrogen bonding under minimal ionic interference. All spectra were collected at room temperature under a purge of dry air.

Although in SEIRAS, the total penetration depth can extend up to ∼70 nm, approximately corresponding to the thickness of the metal film, the local plasmonic field enhancement is confined to the gaps between nanoparticles, which probe ∼5-10 nm from the electrode surface, making the technique highly surface-sensitive.[33,39−44] While the electrical double layer is typically 1-3 nm, as is often considered as the distance from a flat surface, SEIRAS selectively amplifies the signal from interfacial species within the near-field region of the metal electrode, as given by the gaps between nanoparticles. Prior studies demonstrate that spectral features of interfacial species are distinctly observed even when bulk solvent contributions might exist.[45,46] Our spectral analysis follows this precedence, ensuring that the conclusions drawn about interfacial hydrogen bonding and local number density (enrichment) remain valid.

Molecular Dynamics Simulations. Mixtures of 1%, 5%, 10%, and 20% DMSO in water in between two gold electrodes were prepared using the CHARMM-GUI Multicomponent Assembler module.[47−50] Each gold electrode consisted of three layers of (111) faces (624 Au atoms in each electrode). The two electrodes were placed parallel to each other, and perpendicular to the *z*-axis. The initial separation between the electrodes was 10 nm (the separation varied during the equilibration steps) and their dimensions in the x- and *y*-directions were 3.75 and 4.00 nm, respectively. CHARMM36 force field parameters[51] were used for DMSO and a TIP3P model[52] was used for water molecules. The gold atoms were modeled with the Interface force field[53] that is compatible with CHARMM. In addition to setting up this set of systems with parallel electrodes, aqueous systems with the same DMSO and water compositions were also prepared but without the gold electrodes. For the latter, standard NPT simulations at 300 K and 1 atm were performed to obtain the mixtures' densities.

MD simulations for the electrode systems were performed with the LAMMPS software package (version 2 Aug 2023)[54] along with the ELECTRODE package[55] in LAMMPS that implements a constant potential method. During minimization and equilibration, periodic boundary conditions were used in the x- and *y*-directions and non-periodic boundary conditions in the *z*-direction, for which the slab method[56] was applied with a correction factor of 3.0. For each prepared system, a short minimization using a conjugate gradient algorithm was followed by a 2 ns equilibration run where we turn on the constant potential algorithm. In these equilibration runs, one electrode was fixed and the second electrode was allowed to move like a rigid piston along the *z*-direction under the influence of an external pressure of 1 atm. Temperature was maintained at 300 K using a Nosé-Hoover thermostat.[57] For each mixture, two sets of simulations were performed: **1.** The electrode potential was kept at 0 V for both electrodes and **2.** One electrode was set at -0.6 V and the other at +0.6 V. For the equilibration runs, a conjugate gradient minimization algorithm (that allows moving electrodes) was used to obtain the electrode charge at every time step.[58] At the end of these runs we verified that the bulk densities at the center of the simulation box were like the bulk densities obtained in the NPT runs of the same DMSO/water mixtures (with no electrodes) mentioned above. Finally, 12 ns production runs were performed with fixed electrode locations using periodic boundary conditions in all spatial directions using the finite field approach[59,60] as implemented in the ELECTRODE package in LAMMPS. A 2 fs time step was used for equilibration and production runs using SHAKE[61] to constrain molecular bonds. Configurations were saved every 2 ps for analysis. van der Waals interactions were modeled with Lennard-Jones potentials using a 1.2 nm cutoff and the long-range electrostatics interactions were computed with a particle-particle-particle-mesh method[61] with relative accuracy of 10^{-7}. For some of the analysis reported here we used analysis tools from GROMACS software.[62]

In our constant-potential MD simulations, explicit ions were excluded due to the challenges of representing ionic distributions at low concentrations (10 mM) in a simulation box of ∼10 nm. At this ionic strength, only 2−3 ions would be present, introducing statistical noise, artificial periodicity effects and other instabilities. While this approximation neglects the diffuse layer of the EDL, the simulated potential-driven interactions provide insights into solvent structuring and hydrogen bonding near the interface. Future work with larger simulation boxes or enhanced sampling methods could explicitly incorporate ionic effects to fully capture the EDL.

RESULTS AND DISCUSSION

Interfacial H-Bonding Environment Measured by SEIRAS. The S═O stretching region reveals the balance of DMSO−water and DMSO−DMSO interactions at the interface. Quantitative analysis to extract the DMSO H-bonded (HB) and non-bonded populations was performed via a global fitting algorithm of the experimental spectra.[37,63] This procedure fits the spectra to six Gaussian functions that correspond to six distinct populations with the following center frequencies (wavenumbers): 2HB at 1009 cm^{-1}, 1HB at 1022 cm^{-1}, 0HB at 1058 cm^{-1}, aggregate at 1040 cm^{-1}, $-CH_3$ rocking at 1016 cm^{-1}, and aggregate $-CH_3$ rocking at 1034 cm^{-1}. The relative population of each species can be calculated as the ratio of the oscillator-strength corrected areas of each fitted Gaussian profile relative to the total peak areas (excluding the overlapping $-CH_3$ rocking mode). The global fitting procedure is described in detail in Section S2.

We have previously reported the concentration-dependent changes at the interface in comparison to the bulk at OCP. In brief, we showed that DMSO is enriched by a factor of ∼4× at the interface compared to the bulk at low DMSO concentration.[37] In addition, the number of S═O−water H-bonds was reduced at the interface compared to bulk, which points towards the interface being a significantly more hydrophobic environment than the bulk. Here, we focus on the effects of applied potential on the local interfacial environment via both spectroscopy and simulation. Note that for the simulation, the potential is referenced vs the potential of zero charge (PZC). In the experiment, the potentials are measured vs Ag/AgCl (0.198 V vs SHE), which conveniently coincides with the PZC on Au (∼0.2 V vs SHE).[64] Therefore, positive potential in both experiments and simulations in this work translates to positively charged electrode surface, and vice

https://doi.org/10.1021/acselectrochem.4c00175
ACS Electrochem. 2025, 1, 709−717

versa. The changes in lineshapes are relatively small, though the changes can be observed when computing the difference across different potentials (Figure 2, Figures S4-5). The effect

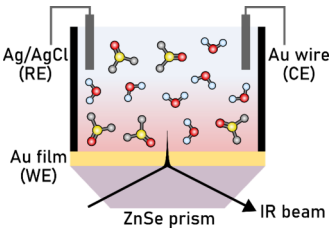

Figure 1. Illustration of the SEIRAS setup for *in situ* spectroelectrochemical measurements of the cosolvent systems. The reference electrode (RE) and counter electrode (CE) are Ag/AgCl and a gold wire, respectively. The gold film is the working electrode (WE). The ZnSe prism is the ATR substrate.

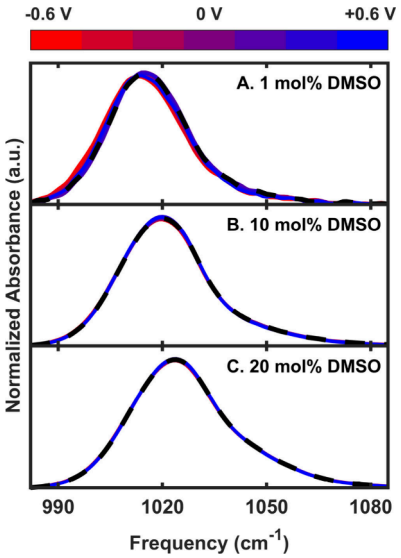

Figure 2. Representative SEIRAS spectra of the S═O stretching region at (A) 1 mol % DMSO, (B) 10 mol % DMSO, and (C) 20 mol % DMSO, at select applied potentials (from −0.6 V, red, to +0.6 V, blue, in steps of 0.2 V) and at 0 V potential (black dashed line). Spectra were normalized by total peak area. Additional spectra at all measured concentrations and applied potentials can be found in Figure S2.

of potential is more pronounced at low concentrations. At negative potentials, the S═O stretch exhibits a minor redshift in center frequency and a higher absorbance. This redshift is more prominent in lower DMSO concentrations and can be attributed to a population increase of more hydrated DMSO molecules at the interface. Conversely, at positive potentials, the S═O stretch appears similar to 0 V at concentrations below 25 mol % DMSO (Figure S4). The full-width at half-maximum values increase with increasing concentration but not with applied potentials (Figure S5).

The H-bond analysis for the S═O group (Figure 3), obtained by fitting the lineshapes, as described above, reveals that the H-bond populations are dependent on the potential. The potential-dependent H-bond populations can be interpreted within three different concentration regimes, despite the error bars being relatively large, trends can nonetheless be observed: **1.** At low concentrations (<10 mol %), negative potentials increase the number of H-bonds at the interface. However, positive potentials (above 0 V) are observed to have only a slight effect on the H-bond populations (Figure 3A-C). **2.** Within the intermediate concentration range (15-30 mol %) there is effectively no change in the number of H-bonds (Figure 3D). **3.** In the high concentration range (>30 mol %), we observe that the trend is reversed compared to the dilute regime, in this case there is a slight decrease in the number of H-bonds at negative potentials (Figure 3E). These non-monotonic trends with voltage and concentrations point towards multiple phenomena contributing to changes in the local environment at the interface.

Next we examine interfacial water by measuring the O−D stretching region of HOD in H_2O (or the O−H stretching mode of HOD in D_2O), which provides direct molecular information on the H-bonding environment of water.[65,66] Figure S8 shows an increase in the O−D stretch absorbance below 10 mol % DMSO at positive potentials. After normalization, the lineshapes show negligible changes from applied potentials (Figure S9). These results indicate that the H-bond populations of water remain nearly unchanged as a function of potential. The limited effect on H-bond populations suggests that DMSO, as a strong hydrogen bond acceptor, stabilizes the interfacial environment, leading to a less pronounced potential-dependent restructuring of water. This is consistent with recent findings on aprotic solvent-modulated interfacial behavior.[46,67] Our results highlight that in mixed DMSO-water systems, DMSO plays a dominant role in defining interfacial solvation environment.

Potential-Dependent Enrichment of Interfacial Molecules. The potential-dependent interfacial enrichment or depletion of DMSO and water be computed from the experimental spectra by taking the ratio of integrated peak areas before normalization (relative to 0 V potential): a relative enrichment value >1 means a larger IR absorbance, or "enrichment", and a value <1 means a lower IR absorbance, or "depletion". Figure 4A shows a general enrichment of DMSO at more negative potentials by at least 5% compared to 0 V at all DMSO concentrations. At 1 mol % DMSO, the largest DMSO relative enrichment is ∼8%, then increases at 3 mol % to ∼13%, and plateaus starting from 20 mol % to ∼5%. At positive applied potentials, the only DMSO relative depletion over 5% is ∼14% at 1 mol % DMSO. On the other hand, water is enriched at more negative potentials (−0.6 V) and only at concentrations below 10 mol % DMSO (Figure 4B), with highest enrichment ∼17% at 0 mol %. Water does not exhibit any interfacial depletion with applied potential below 30 mol %.

One possible interpretation for an increase in IR absorbance (or enrichment) with an applied potential is an increase in the population of that specific species at the interface. Another possible explanation for the changes in IR signal is molecular reorientation in the interfacial region. SEIRAS is a surface-sensitive and orientation-selective technique. In SEIRAS, the plasmonically enhanced field is predominantly oriented along the gaps between nanoparticles (i.e. perpendicular to the gold nanoparticle surface), making only those vibrational modes with transition dipole moments (TDM) perpendicular to the surface contributing to the largest spectroscopic signal.[40,42,68] One limitation of SEIRAS, unlike traditional attenuated total internal reflection spectroscopy, is that polarization does not allow for directly measuring the orientation of molecules.[33,40,42,68] However, both the change in population and molecular reorientation could be concurrent with applied potential. While the effects of potential are relatively modest,

https://doi.org/10.1021/acselectrochem.4c00175
ACS Electrochem. 2025, 1, 709−717

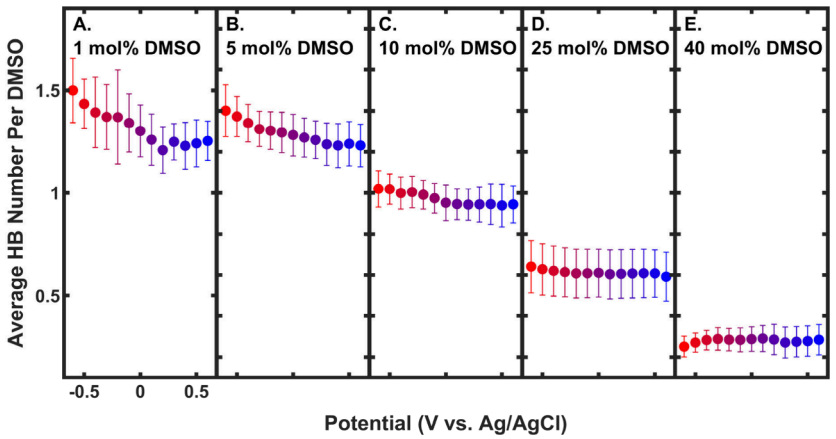

Figure 3. Average H-bonding (HB) number per DMSO molecule at the gold electrode as a function of applied potential (−0.6 V in red to +0.6 V in blue) at select dilute (1, 5, 10 mol % DMSO, panels A−C) and concentrated (25, 40 mol % DMSO, panels D, E) compositions. The error bars represent standard deviation calculated from the global fitting procedure. Additional spectra at all measured concentrations and applied potentials can be found in Figure S10.

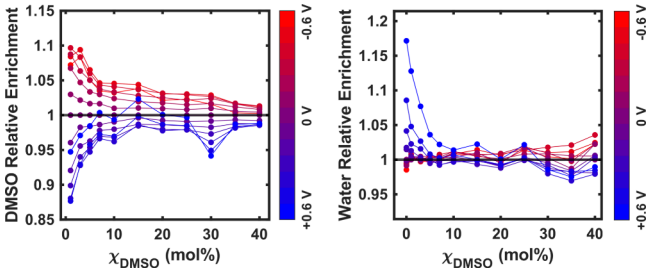

Figure 4. Relative enrichment of DMSO (left panel) and water (right panel) at the gold electrode at applied potentials (−0.6 V in bright red to +0.6 V in bright blue) as a function of DMSO mol % compared to 0 V potential conditions. The potential values are relative to the Ag/AgCl reference electrode. The enrichment was calculated as the ratio of the peak area at applied potentials to the peak area without an applied potential. Note: the DMSO mol % values in the left and right panels start at 1 mol % and 0 mol %, respectively.

showing a ∼10% modulation of the signal, with most pronounced changes at the lowest concentrations, these changes are relatively small compared to the overall enrichment effects of concentration, which in DMSO we observed to be 200-400% enrichment at the surface. Nonetheless, this study shows that changes in potential can affect the interface, despite species being uncharged.

Interpretation Derived from Constant-Potential MD Simulations. Spectroscopic observations suggest that electrode potential modulates the interfacial H-bond networks, whether by changing the DMSO-water ratios, or by stabilizing specific molecular configurations, such as local orientations. We interpret these changes by performing constant-potential MD simulations. In these simulations, the gold atoms are assigned initial charges, which are then re-optimized throughout the simulation to maintain a constant potential between electrodes in respond to the molecules reorganizing around the surface. This enables the surface to "respond" to changes in the cosolvent molecules, as the electrode responds in the experimental system. Simulations are carried out at three different potentials, 0 V, −0.6 V and +0.6 V, thus enabling us to compare the results extracted from MD trajectories with experimental observables. A snapshot of the MD box is included in Figure S34 for illustration purposes.

Similar to experiments, H-bond populations, computed from MD simulations (Figure 5), also exhibit differences between

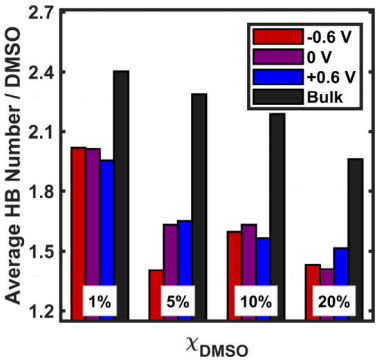

Figure 5. Average H-bond (HB) number per DMSO molecule as a function of DMSO concentration at applied potentials. The black bars represent the average number of H-bonds in bulk, and the (red, purple, and blue) bars represent interfacial populations at −0.6, 0, and +0.6 V, respectively. For the applied potential systems, the error estimates by block averaging are <0.05 (in units of H-bond numbers) for the 1% and 5% mixtures and <0.2 for the 10% and 20% mixtures. For the H-bond numbers in the bulk the errors are <0.001.

the bulk and the interfacial environments, and in addition, simulations show that potential affects relative H-bond populations of DMSO at the interface. The changes in bulk vs interface can be compared with previous results under open circuit potential.[37] Qualitatively, the current MD simulations are consistent with previous results, showing dehydration at the interface, the H-bond populations are consistent with previous experiments and also generally consistent with previous fixed-charge MD simulations.[37] This is expected, given that the MD force fields were the same as the previous simulations. The key difference is that the present MD simulations are constant-potential MD simulations, with fluctuating charges on the gold atoms, compared to previous simulations without charges on the gold atoms.[37] The constant-potential MD simulations account for electrode polarization, and thus are expected to more accurately reproduce the environment at the interface.

https://doi.org/10.1021/acselectrochem.4c00175
ACS Electrochem. 2025, 1, 709−717

The effects of potential on H-bond populations can be observed by comparing the MD trajectories for positive, neutral, and negative potentials (Figure 5). The effect of potential on H-bond populations is relatively small compared to the populations in bulk versus surface, nonetheless the simulation results are consistent with experiment: simulations show that at low DMSO concentrations (1 mol %), negative potentials increase the number of hydrogen bonds compared to positive potentials. Higher concentrations (20 mol %) show an increase in the number of H-bonds at positive potentials.

The DMSO enrichment at the interface (Figure 6) is significantly greater compared to experiments, with simulations

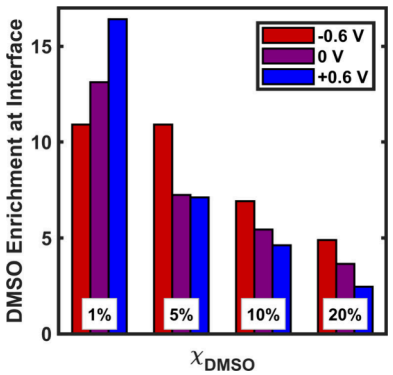

Figure 6. DMSO enrichment at the gold electrode at applied potentials (0 V in purple, −0.6 V in red, +0.6 V in blue) as a function of DMSO mol % from MD simulations. Error estimates obtained by block averaging are smaller than 0.8.

showing a ∼12-fold enrichment versus the bulk and experiments showing a ∼4-fold enrichment at the lowest DMSO concentrations.[37] This means that when the bulk concentration is 1 mol % DMSO, experiments predict that the interface contains 4 mol % DMSO, and simulations show a 12 mol % DMSO concentration. As observed from H-bond populations in bulk experiments, this change in concentration can lead to significant changes in H-bond populations.

This strong interfacial enrichment of DMSO at 1 mol % DMSO concentration, leading to near-complete depletion of DMSO from the bulk (Figure S39) is consistent with prior experimental and computational studies that show DMSO preferentially adsorbs onto metal surfaces due to strong dipole-surface interactions.[3,4,37,63] However, we understand that in a larger simulation box, some bulk-phase DMSO molecules will remain once the surface is saturated, which could allow for improved statistical sampling of bulk-like behavior. While this does not alter the qualitative trends observed in potential-dependent enrichment and hydrogen bonding, we note that the absence of bulk-phase DMSO in small-scale simulations may amplify interfacial effects, particularly at the lowest DMSO concentrations. Future studies with larger system sizes or enhanced sampling techniques will further assess this behavior to ensure that simulation box limitations do not introduce unintended artifacts.

Next, we can examine the effects of interfacial potential on the molecular orientations. Figures S35-38 show the concentration-dependent average water dipole orientations as a function of distance from the electrode surface for positive, neutral, and negative interfaces. In addition, Figures S39-40 show the orientation of DMSO molecules. Generally, we observe that potential does not significantly impact the orientations of DMSO, however, water orientations are significantly altered as a result of applied potential. Without potential, the net orientation is perpendicular to the surface, as discussed in previously where water molecules are observed to assume a "buckled" configuration.[37] Once the potential is turned on, strong preferential orientation is observed throughout the box. Near the surface, at negative potential we observe particularly strong reorientation of water molecules across all DMSO concentrations in agreement with previous studies on potential-dependent water structuring.[35,69] For instance, at 1% the dipole projection in pure water is approximately 0, and this value increases to ∼0.3 indicating that on average the water molecules adopt an angle of ∼73° suggesting that the HER process could be significantly altered given the strong reorientation of water near the interface. Positive potential does not appear to reorient water as strongly. This is consistent with the effects on H-bond populations (Figure 3), where positive potentials appear to have a more moderate effect compared to negative potentials. It is worth noting that SEIRAS is not able to directly access orientational information, however, the relatively unchanged spectral features of water, suggests that orientational effects do not significantly influence the measurements. In contrast, DMSO orientations remain relatively unchanged, suggesting its preferential adsorption and stabilizing effect on the interfacial H-bonding network are the primary drivers of the changes in H-bond populations. This indicates that while water molecules respond dynamically to the applied potential, DMSO modulates the extent of these changes by altering the local solvation environment and H-bonding network at the electrode interface.

The impact of aprotic solvents on interfacial hydrogen bonding and their role in inhibiting HER has been previously demonstrated in the context of CO_2 reduction, where solvents such as DMF were found to alter interfacial water organization and improve faradaic efficiency.[46,70−72] Our findings on DMSO similarly indicate that its presence at the electrode interface modulates H-bonding, with implications for using these effects to control electrochemical reactivity. Therefore, our study examines how applied potential influences solvent structure and hydrogen bonding instead of the direct effects of electrolyte ions, which are also present and can significantly impact electrocatalytic processes. SEIRAS experiments show clear potential-dependent changes, even at low electrolyte concentrations, confirming that solvent−solvent interactions and electrostatic potential primarily dictate interfacial reorganization. While our MD simulations exclude explicit counterions, they capture key electrostatic interactions, that are consistent with experiments. We acknowledge that at higher electrolyte concentrations, counterions could play a larger role, and future studies incorporating explicit ionic models could provide more quantitative insights into their impact on the electrode interface.

Overall, MD simulations are consistent with SEIRAS measurements, showing that the effect of potential on enrichment is relatively moderate, and that the strongest effects are represented by the dipole orientations, particularly with respect to water. The non-monotonic changes in H-bond populations across DMSO concentrations are also consistent between experiment and simulation. We have identified the most important factors that drive changes in H-bond populations, namely the enrichment of DMSO and reorientation of water molecules.

https://doi.org/10.1021/acselectrochem.4c00175
ACS Electrochem. 2025, 1, 709−717

In summary, SEIRAS reveals concentration and potential-dependent changes in the S═O H-bond populations. There is a notable decrease in DMSO H-bond populations with increasing DMSO concentration, as DMSO disrupts the donor−acceptor balance of water. Interestingly, we observed potential-dependent changes in populations for a given DMSO concentration), despite the species being electrically neutral. Specifically, within lower concentrations and negative potentials, the H-bond populations are increased, possibly due to fewer DMSO−DMSO interactions and more DMSO−water interactions related to the strong effect of potential on interfacial water orientations. Furthermore, within negative potentials DMSO molecules become enriched at the surface. At low concentrations (e.g., 1 mol %), DMSO enriches up to ∼8% compared to 0 V. As the concentration increases from 3 mol % to 20 mol %, enrichment peaks around 13% before stabilizing, suggesting surface saturation. This is because, at more negative potentials, the surface of the gold electrode is likely more electron-rich, which could lead to stronger interactions between the electrode and solvent molecules. These stronger interactions disrupt the interfacial H-bond networks, potentially decreasing the average H-bond number. Within the higher concentration regime, the average H-bond number becomes less dependent on the applied potentials, indicating that the system becomes less sensitive to changes in the potential, possibly because water becomes a lesser component of the solution, and changes in water orientation are less pronounced. Within the high concentration regime, DMSO−DMSO interactions dominate, and the average number of H-bonds per DMSO molecule is lower and relatively constant across the applied potential range. The stabilization seen here suggests that the H-bonding network reaches a limit where additional DMSO molecules do not significantly change the overall hydrogen bonding environment.

Above 20 mol %, enrichment reaches ∼5%, indicating a balanced distribution between DMSO and water. This enrichment of DMSO at the negatively charged surface (Figures S45−S46) is likely due to the electrostatic interactions between the polar DMSO molecules and the negatively charged electrode. DMSO has a large dipole moment, with a partial positive charge on the sulfur atom and partial negative charges on the oxygen atoms. This polarity makes DMSO molecules more likely to align with the negatively charged surface. At positive potentials (+0.6 V), there is a depletion of DMSO at the interface, particularly at low concentrations (∼14% depletion at 1 mol %). As concentration increases, depletion lessens, though some DMSO remains at higher concentrations (Figures S41−S44). This is likely due to repulsion from the positively charged surface, causing DMSO displacement.

CONCLUSIONS AND OUTLOOK

In conclusion, we have characterized the H-bond populations and enrichment of water and DMSO across a range of electrode polarization (potentials) and concentrations. This study demonstrates that electrically neutral DMSO molecules can significantly modulate water H-bond network at the gold-solution interface. SEIRAS and constant potential MD simulation show that at negative potential DMSO become enriched at the interface (or depleted from the bulk), especially at lower DMSO concentrations with increased H-bond population. Conversely, at higher DMSO concentrations, DMSO−DMSO interactions dominates and the solvation structure becomes less sensitive to the applied potential.

These findings provide an essential foundation for understanding electrochemical catalytic reactions in water such as the HER or CO_2 reduction by manipulating cosolvent composition and electrode polarization. In general, characterizing the H-bond networks provides a more complete picture for incorporating these effects into modeling and optimizing electrocatalytic processes at the interface. While the present study provides an initial characterization of interfacial H-bond ensembles, further studies will incorporate H-bond dynamics, measuring the effects of potential on the H-bond lifetime at the interface.

ASSOCIATED CONTENT

Data Availability Statement

The data supporting this article have been included as part of the Supplementary Information.

Supporting Information

The Supporting Information is available free of charge at https://pubs.acs.org/doi/10.1021/acselectrochem.4c00175.

Infrared spectra of the S═O stretch mode and the corresponding frequency shift, changes in fwhm, average H-bond number per DMSO molecule as a function of applied potential, comparison of the absolute value of the slopes calculated from the linear fit of average H-bond number per DMSO molecule, O−D stretching region as a function of applied potential, global fitting of the S═O stretch mode to sum of Gaussian functions, S═O H-bond population as a function of applied potential, average orientation distribution of water and DMSO molecules and number density for various interactions obtained from the molecular dynamics simulation, cyclic voltammogram of N_2-purged 10 mM $KClO_4$ and 0.1 M phosphate buffer on Au film on ZnSe prism and Au disk (PDF)

AUTHOR INFORMATION

Corresponding Author

Carlos R. Baiz − *Department of Chemistry, University of Texas at Austin, Austin, Texas 78712, United States;* orcid.org/0000-0003-0699-8468; Email: cbaiz@cm.utexas.edu

Authors

Saptarsi Mondal − *Department of Chemistry, University of Texas at Austin, Austin, Texas 78712, United States*

Ziareena A. Al-Mualem − *Department of Chemistry, University of Texas at Austin, Austin, Texas 78712, United States;* orcid.org/0000-0001-9857-5360

Alfredo E. Cardenas − *The Oden Institute for Computational Engineering and Sciences, University of Texas at Austin, Austin, Texas 78712, United States;* orcid.org/0000-0002-9687-7979

Sulagna Hazarika − *Department of Chemistry, University of Texas at Austin, Austin, Texas 78712, United States*

Hyein Lee − *Department of Chemistry, University of Texas at Austin, Austin, Texas 78712, United States*

Hang Ren − *Department of Chemistry, University of Texas at Austin, Austin, Texas 78712, United States;* orcid.org/0000-0002-9480-8881

Complete contact information is available at:

https://doi.org/10.1021/acselectrochem.4c00175
ACS Electrochem. 2025, 1, 709−717

https://pubs.acs.org/10.1021/acselectrochem.4c00175

Author Contributions

S.M. and Z.A.A.-M. contributed equally.

Notes

The authors declare no competing financial interest.

■ ACKNOWLEDGMENTS

This project was funded by the U.S. Department of Energy (DE-SC0023221) and the Welch Foundation (F-1891 to C.R.B. and F-2158 to H.R.). C.R.B. thanks the Alfred P. Sloan Foundation for their support. Z.A.A. was funded by a UT Austin Provost's Graduate Excellence Fellowship. Part of the simulations were carried out at the Texas Advanced Computing Center (TACC). The authors thank Keegan Lorenz-Ochoa for insightful discussions.

■ REFERENCES

(1) Schmickler, W.; Santos, E. *Interfacial Electrochemistry*; Springer Berlin Heidelberg, 2010.
(2) Koper, M. T. M. Theory of multiple proton−electron transfer reactions and its implications for electrocatalysis. *Chem. Sci.* **2013**, *4* (7), 2710−2723.
(3) Dubouis, N.; Serva, A.; Berthin, R.; Jeanmairet, G.; Porcheron, B.; Salager, E.; Salanne, M.; Grimaud, A. Tuning water reduction through controlled nanoconfinement within an organic liquid matrix. *Nat. Catal.* **2020**, *3* (8), 656−663.
(4) Wang, T.; Zhang, Y.; Huang, B.; Cai, B.; Rao, R. R.; Giordano, L.; Sun, S.-G.; Shao-Horn, Y. Enhancing oxygen reduction electrocatalysis by tuning interfacial hydrogen bonds. *Nat. Catal.* **2021**, *4* (9), 753−762.
(5) Bonn, M.; Nagata, Y.; Backus, E. H. G. Molecular Structure and Dynamics of Water at the Water−Air Interface Studied with Surface-Specific Vibrational Spectroscopy. *Angew. Chem., Int. Ed.* **2015**, *54* (19), 5560−5576.
(6) Shen, Y. R. Surface properties probed by second-harmonic and sum-frequency generation. *Nature* **1989**, *337* (6207), 519−525.
(7) Gomes, R. J.; Kumar, R.; Fejzić, H.; Sarkar, B.; Roy, I.; Amanchukwu, C. V. Modulating water hydrogen bonding within a non-aqueous environment controls its reactivity in electrochemical transformations. *Nat. Catal.* **2024**, *7* (6), 689−701.
(8) Xu, K. Nonaqueous liquid electrolytes for lithium-based rechargeable batteries. *Chem. Rev.* **2004**, *104* (10), 4303−4417.
(9) Al-Mualem, Z. A.; Lorenz-Ochoa, K. A.; Pan, L.; Ren, H.; Baiz, C. R. Controlling Interfacial Hydrogen Bonding at a Gold Surface: The Effect of Organic Cosolvents. *J. Phys. Chem. Lett.* **2024**, *15*, 4391−4399.
(10) Oh, K.-I.; Rajesh, K.; Stanton, J. F.; Baiz, C. R. Quantifying hydrogen-bond populations in DMSO/water mixtures. *Angew. Chem., Int. Ed. Engl.* **2017**, *129*, 11533−11537.
(11) Liang, E.; Verma, V.; Guo, M.; Jia, L.; Guinn, E. J.; Heng, J. Y. Y. Sequence-dependent dipeptide solubility in ethanol-water and DMSO-water solutions. *J. Mol. Liq.* **2024**, *402*, 124742.
(12) Wang, C.; Kuang, B.; Wang, S.; Sun, C. Intermolecular competition regulates hydrogen bond reorientation in DMSO-Water: Insights from Raman scattering. *J. Mol. Liq.* **2024**, *396*, 124041.
(13) Yan, Y.; Zhang, J.; Chen, L.; Ren, G.; Zhou, L.; Liu, L.; Zhang, X.; Ouyang, C.; Wang, H.; Han, J. Interactions between ions and water-DMSO mixed solvent. *J. Mol. Liq.* **2024**, *414*, 126204.
(14) Scherer, J. R.; Go, M. K.; Kint, S. Raman spectra and structure of water in dimethyl sulfoxide. *J. Phys. Chem.* **1973**, *77* (17), 2108−2117.
(15) Allen, H. C.; Gragson, D. E.; Richmond, G. L. Molecular structure and adsorption of dimethyl sulfoxide at the surface of aqueous solutions. *J. Phys. Chem. B* **1999**, *103* (4), 660−666.
(16) Shikata, T.; Sugimoto, N. Dimeric Molecular Association of Dimethyl Sulfoxide in Solutions of Nonpolar Liquids. *J. Phys. Chem. A* **2012**, *116* (3), 990−999.
(17) Hazra, M. K.; Bagchi, B. Non-equilibrium solvation dynamics in water-DMSO binary mixture: Composition dependence of non-linear relaxation. *J. Chem. Phys.* **2018**, *149* (8), 084501.
(18) Harpham, M. R.; Levinger, N. E.; Ladanyi, B. M. An investigation of water dynamics in binary mixtures of water and dimethyl sulfoxide. *J. Phys. Chem. B* **2008**, *112* (2), 283−293.
(19) Oh, K. I.; You, X.; Flanagan, J. C.; Baiz, C. R. Liquid-Liquid Phase Separation Produces Fast H-Bond Dynamics in DMSO-Water Mixtures. *J. Phys. Chem. Lett.* **2020**, *11* (5), 1903−1908.
(20) Wong, D. B.; Sokolowsky, K. P.; El-Barghouthi, M. I.; Fenn, E. E.; Giammanco, C. H.; Sturlaugson, A. L.; Fayer, M. D. Water dynamics in water/DMSO binary mixtures. *J. Phys. Chem. B* **2012**, *116* (18), 5479−5490.
(21) Banik, D.; Kundu, N.; Kuchlyan, J.; Roy, A.; Banerjee, C.; Ghosh, S.; Sarkar, N. Picosecond solvation dynamics - A potential viewer of DMSO - Water binary mixtures. *J. Chem. Phys.* **2015**, *142* (5), 054505.
(22) Lotze, S.; Groot, C. C. M.; Vennehaug, C.; Bakker, H. J. Femtosecond mid-infrared study of the dynamics of water molecules in water-acetone and water-dimethyl sulfoxide mixtures. *J. Phys. Chem. B* **2015**, *119* (16), 5228−5239.
(23) Luzar, A.; Chandler, D. Structure and hydrogen bond dynamics of water−dimethyl sulfoxide mixtures by computer simulations. *J. Chem. Phys.* **1993**, *98* (10), 8160−8173.
(24) Perera, A.; Mazighi, R. On the nature of the molecular ordering of water in aqueous DMSO mixtures. *J. chem. Phys.* **2015**, *143* (15), 154502.
(25) Oh, K.-I.; Baiz, C. R. Molecular heterogeneity in aqueous cosolvent systems. *J. chem. Phys.* **2020**, *152* (19), 190901−190901.
(26) Bockris, J. O. M.; Reddy, A. K. N. *Modern Electrochemistry 2B: Electrodics in Chemistry, Engineering, Biology and Environmental Science*; Springer, 1998.
(27) Ryan, M. J.; Yang, N.; Kwac, K.; Wilhelm, K. B.; Chi, B. K.; Weix, D. J.; Cho, M.; Zanni, M. T. The hydrogen-bonding dynamics of water to a nitrile-functionalized electrode is modulated by voltage according to ultrafast 2D IR spectroscopy. *Proc. Natl. Acad. Sci. U. S. A.* **2023**, *120* (52), No. e2314998120.
(28) Ataka, K.-i.; Osawa, M. In Situ Infrared Study of Water−Sulfate Coadsorption on Gold(111) in Sulfuric Acid Solutions. *Langmuir* **1998**, *14* (4), 951−959.
(29) Aguirre, A.; Berli, C. L. A.; Collins, S. E. ATR-FTIR spectrokinetic analysis of the CO adsorption and oxidation at water/platinum interface. *Catal. Today* **2017**, *283*, 127−133.
(30) Kas, R.; Ayemoba, O.; Firet, N. J.; Middelkoop, J.; Smith, W. A.; Cuesta, A. In-Situ Infrared Spectroscopy Applied to the Study of the Electrocatalytic Reduction of CO2: Theory, Practice and Challenges. *ChemPhysChem* **2019**, *20* (22), 2904−2925.
(31) Delley, M. F.; Nichols, E. M.; Mayer, J. M. Interfacial Acid-Base Equilibria and Electric Fields Concurrently Probed by in Situ Surface-Enhanced Infrared Spectroscopy. *J. Am. Chem. Soc.* **2021**, *143* (28), 10778−10792.
(32) Ataka, K.; Kottke, T.; Heberle, J. Thinner, smaller, faster: IR techniques to probe the functionality of biological and biomimetic systems. *Angew. Chem., Int. Ed.* **2010**, *49* (32), 5416−5424.
(33) Kozuch, J.; Ataka, K.; Heberle, J. Surface-enhanced infrared absorption spectroscopy. *Nat. Rev. Methods Primers* **2023**, *3* (1), 1−19.
(34) Angerstein-Kozlowska, H.; Conway, B. E.; Hamelin, A.; Stoicoviciu, L. Elementary steps of electrochemical oxidation of single-crystal planes of Au Part II. A chemical and structural basis of oxidation of the (111) plane. *J. Electroanal. Chem.* **1987**, *228* (1-2), 429−453.
(35) Ataka, K. I.; Yotsuyanagi, T.; Osawa, M. Potential-dependent reorientation of water molecules at an electrode/electrolyte interface studied by surface-enhanced infrared absorption spectroscopy. *J. Phys. Chem.* **1996**, *100* (25), 10664−10672.

(36) Bao, W. J.; Li, J. J.; Li, J. J.; Zhang, Q. W.; Liu, Y.; Shi, C. F.; Xia, X. H. Au/ZnSe-Based Surface Enhanced Infrared Absorption Spectroscopy as a Universal Platform for Bioanalysis. *Anal. Chem.* **2018**, *90* (6), 3842−3848.
(37) Al-Mualem, Z. A.; Lorenz-Ochoa, K. A.; Pan, L.; Ren, H.; Baiz, C. R. Controlling Interfacial Hydrogen Bonding at a Gold Surface: The Effect of Organic Cosolvents. *J. Phys. Chem. Lett.* **2024**, *15* (16), 4391−4399.
(38) Rodríguez, O.; Pence, M. A.; Rodríguez-López, J. Hard Potato: A Python Library to Control Commercial Potentiostats and to Automate Electrochemical Experiments. *Anal. Chem.* **2023**, *95* (11), 4840−4845.
(39) Osawa, M.; Ataka, K.-i. Electromagnetic mechanism of enhanced infrared absorption of molecules adsorbed on metal island films. *Surf. Sci. Lett.* **1992**, *262* (3), L118−L122.
(40) Kozuch, J.; Ataka, K.; Heberle, J. Surface-enhanced infrared absorption spectroscopy. *Nat. Rev. Methods Primers* **2023**, *3* (1), 70.
(41) Ataka, K.; Stripp, S. T.; Heberle, J. Surface-enhanced infrared absorption spectroscopy (SEIRAS) to probe monolayers of membrane proteins. *Biochim. Biophys. Acta* **2013**, *1828* (10), 2283−2293.
(42) Hartstein, A.; Kirtley, J. R.; Tsang, J. C. Enhancement of the infrared absorption from molecular monolayers with thin metal overlayers. *Phys. Rev. Lett.* **1980**, *45* (3), 201−204.
(43) Heberle, J.; Ataka, K. Surface Enhanced Infrared Absorption Spectroscopy. In *Encyclopedia of Biophysics*, Roberts, G. C. K., Ed.; Springer Berlin Heidelberg, 2013; pp 2528−2531.
(44) Griffiths, P. R. Surface-enhanced infrared absorption spectroscopy: principles and applications. In *Spectroscopic Properties of Inorganic and Organometallic Compounds: Techniques, Materials and Applications*, Yarwood, J., Douthwaite, R., Duckett, S., Eds.; Vol. *44*; The Royal Society of Chemistry, 2013; pp 95−122.
(45) Yamakata, A.; Osawa, M. Destruction of the Hydration Shell around Tetraalkylammonium Ions at the Electrochemical Interface. *J. Am. Chem. Soc.* **2009**, *131* (20), 6892−6893.
(46) Mohandas, N.; Narayanan, T. N.; Cuesta, A. Tailoring the Interfacial Water Structure by Electrolyte Engineering for Selective Electrocatalytic Reduction of Carbon Dioxide. *ACS Catal.* **2023**, *13* (13), 8384−8393.
(47) Jo, S.; Kim, T.; Iyer, V. G.; Im, W. CHARMM-GUI: A web-based graphical user interface for CHARMM. *J. Comput. Chem.* **2008**, *29* (11), 1859−1865.
(48) Lee, J.; Cheng, X.; Swails, J. M.; Yeom, M. S.; Eastman, P. K.; Lemkul, J. A.; Wei, S.; Buckner, J.; Jeong, J. C.; Qi, Y.; et al. CHARMM-GUI Input Generator for NAMD, GROMACS, AMBER, OpenMM, and CHARMM/OpenMM Simulations Using the CHARMM36 Additive Force Field. *J. Chem. Theory Comput.* **2016**, *12* (1), 405−413.
(49) Choi, Y. K.; Kern, N. R.; Kim, S.; Kanhaiya, K.; Afshar, Y.; Jeon, S. H.; Jo, S.; Brooks, B. R.; Lee, J.; Tadmor, E. B.; et al. CHARMM-GUI Nanomaterial Modeler for Modeling and Simulation of Nanomaterial Systems. *J. Chem. Theory Comput.* **2022**, *18* (1), 479−493.
(50) Kern, N. R.; Lee, J.; Kyo Choi, Y.; Im, W. CHARMM-GUI multicomponent assembler for modeling and simulation of complex multicomponent systems. *Biophys. J.* **2022**, *121* (3), 529a−529a.
(51) Huang, J.; Rauscher, S.; Nawrocki, G.; Ran, T.; Feig, M.; De Groot, B. L.; Grubmüller, H.; MacKerell, A. D. CHARMM36m: An improved force field for folded and intrinsically disordered proteins. *Nat. Methods* **2017**, *14* (1), 71−73.
(52) Jorgensen, W. L.; Chandrasekhar, J.; Madura, J. D.; Impey, R. W.; Klein, M. L. Comparison of simple potential functions for simulating liquid water. *J. Chem. Phys.* **1983**, *79* (2), 926−935.
(53) Heinz, H.; Vaia, R. A.; Farmer, B. L.; Naik, R. R. Accurate simulation of surfaces and interfaces of face-centered cubic metals using 12-6 and 9-6 lennard-jones potentials. *J. Phys. Chem. C* **2008**, *112* (44), 17281−17290.
(54) Thompson, A. P.; Aktulga, H. M.; Berger, R.; Bolintineanu, D. S.; Brown, W. M.; Crozier, P. S.; in 't Veld, P. J.; Kohlmeyer, A.; Moore, S. G.; Nguyen, T. D.; et al. LAMMPS - a flexible simulation tool for particle-based materials modeling at the atomic, meso, and continuum scales. *Comput. Phys. Commun.* **2022**, *271*, 108171−108171.
(55) Ahrens-Iwers, L. J. V.; Janssen, M.; Tee, S. R.; Meißner, R. H. ELECTRODE: An electrochemistry package for atomistic simulations. *J. Chem. Phys.* **2022**, *157* (8), DOI: 10.1063/5.0099239.
(56) Yeh, I. C.; Berkowitz, M. L. Ewald summation for systems with slab geometry. *J. Chem. Phys.* **1999**, *111* (7), 3155−3162.
(57) Shinoda, W.; Shiga, M.; Mikami, M. Rapid estimation of elastic constants by molecular dynamics simulation under constant stress. *Physical Review B - Condensed Matter and Materials Physics* **2004**, *69* (13). DOI: 10.1103/PhysRevB.69.134103
(58) Reed, S. K.; Lanning, O. J.; Madden, P. A. Electrochemical interface between an ionic liquid and a model metallic electrode. *J. Chem. Phys.* **2007**, *126* (8). DOI: 10.1063/1.2464084
(59) Dufils, T.; Jeanmairet, G.; Rotenberg, B.; Sprik, M.; Salanne, M. Simulating Electrochemical Systems by Combining the Finite Field Method with a Constant Potential Electrode. *Phys. Rev. Lett.* **2019**, *123* (19), 195501.
(60) Tee, S. R.; Searles, D. J. Fully periodic, computationally efficient constant potential molecular dynamics simulations of ionic liquid supercapacitors. *J. Chem. Phys.* **2022**, *156* (18). DOI: 10.1063/5.0086986
(61) Ryckaert, J.-P.; Ciccotti, G.; Berendsen, H. J. C. Numerical integration of the cartesian equations of motion of a system with constraints: molecular dynamics of n-alkanes. *J. Comput. Phys.* **1977**, *23* (3), 327−341.
(62) Van Der Spoel, D.; Lindahl, E.; Hess, B.; Groenhof, G.; Mark, A. E.; Berendsen, H. J. C. GROMACS: Fast, flexible, and free. *J. Comput. Chem.* **2005**, *26* (16), 1701−1718.
(63) Oh, K.-I.; Rajesh, K.; Stanton, J. F.; Baiz, C. R. Quantifying Hydrogen-Bond Populations in Dimethyl Sulfoxide/Water Mixtures. *Angew. Chem., Int. Ed.* **2017**, *56* (38), 11375−11379.
(64) Silva, F.; Sottomayor, M. J.; Hamelin, A. The temperature coefficient of the potential of zero charge of the gold single-crystal electrode/aqueous solution interface: Possible relevance to gold-water interactions. *J. Electroanal. Chem. Interface Electrochem.* **1990**, *294* (1), 239−251.
(65) Auer, B.; Kumar, R.; Schmidt, J. R.; Skinner, J. L. Hydrogen bonding and Raman, IR, and 2D-IR spectroscopy of dilute HOD in liquid D2O. *Proc. Natl. Acad. Sci. U.S.A.* **2007**, *104* (36), 14215−14220.
(66) Davis, J. G.; Gierszal, K. P.; Wang, P.; Ben-Amotz, D. Water structural transformation at molecular hydrophobic interfaces. *Nature* **2012**, *491* (7425), 582−585.
(67) Gunasekaran, P.; Du, X.; Burley, A.; Le, J.; Cheng, J.; Cuesta, A. Water at electrode−electrolyte interfaces: combining HOD vibrational spectra with ab initio-molecular dynamics simulations. *Chem. Sci.* **2024**, *15* (42), 17469−17480.
(68) Osawa, M.; Ataka, K.-I.; Yoshii, K.; Nishikawa, Y. Surface-Enhanced Infrared Spectroscopy: The Origin of the Absorption Enhancement and Band Selection Rule in the Infrared Spectra of Molecules Adsorbed on Fine Metal Particles. *Appl. Spectrosc.* **1993**, *47* (9), 1497−1502.
(69) Toney, M. F.; Howard, J. N.; Richer, J.; Borges, G. L.; Gordon, J. G.; Melroy, O. R.; Wiesler, D. G.; Yee, D.; Sorensen, L. B. Voltage-dependent ordering of water molecules at an electrode−electrolyte interface. *Nature* **1994**, *368* (6470), 444−446.
(70) Sharifi Golru, S.; Biddinger, E. J. Effect of additives in aqueous electrolytes on CO2 electroreduction. *Chem. Eng. J.* **2022**, *428*, 131303.
(71) Ge, W.; Zhu, Y.; Wang, H.; Jiang, H.; Li, C. Anionic Surfactant-Tuned Interfacial Water Reactivity Promoting Electrocatalytic CO2 Reduction. *ACS Catal.* **2024**, *14* (23), 18156−18166.
(72) Ge, W.; Dong, L.; Wang, C.; Zhu, Y.; Liu, Z.; Jiang, H.; Li, C. Modulating Interfacial Hydrogen-Bond Environment by Electrolyte Engineering Promotes Acidic CO2 Electrolysis. *ACS Catal.* **2024**, *14* (14), 10529−10537.